

EFFECTS OF CURING CONDITIONS ON CRACK BRIDGING RESPONSE OF PVA REINFORCED CEMENTITIOUS MATRIX

E. Esmaeeli[†], J. A. O. Barros^{*}, M. Mastali^{**}

ISISE, Dep. Civil Eng., School Eng., University of Minho
Campus de Azurém 4800-058 Guimarães, Portugal

[†] e-mail: esmaeeli@civil.uminho.pt; ^{*} e-mail: barros@civil.uminho.pt; ^{**} e-mail: m.mastali@civil.uminho.pt

Keywords: strain hardening cementitious composite; PVA fibers; curing effect; fibers crack bridging response.

Summary: *The effect of the different curing conditions on the response of fiber crack bridging of PVA-ECC is studied. The self compacting PVA-ECC was cast into the moulds to produce four similar rectangular panels. These panels were kept under different curing conditions for 28 days. The tensile specimens were cut from these panels, and after executing a notch they were tested under tensile loading. The stress versus crack opening relationship for the specimens extracted from panels cured at different conditions is obtained, and the derived results are compared. The dispersion of results, the stress at crack initiation, the maximum fibers bridging stress and the corresponding crack opening, the absorbed energy and the fibers bridging stiffness are the investigated parameters. Also macroscopic images of the fibers in fracture surface are used to interpret the obtained data. As a result of this study a significant influence of different curing conditions on the fiber crack bridging response was observed.*

1 INTRODUCTION

Tailoring of strain hardening cementitious composites (SHCCs) has been intensively studied during the last decade in order to obtain reliable knowledge for the use of SHCCs in field applications [1-4]. Although the mechanical characteristics of these composites (high ductility and durability) are a distinctive point of interest, the economical aspects were always an obstacle for a larger applicability of this structural material. To achieve a certain level of tensile ductility, the type(s), geometry and volume of the required fibers are the main parameters affecting the costs of SHCCs. This is clearly evident when considering the preliminary generations of SHCCs such as CARDIF[5, 6], Ductal [7] and SIFCON [8]. As an example, in the case of SIFCON a strain hardening capacity (tensile strain at peak tensile stress) of around 1.25% could only be obtained when 12% of steel fibers in the volume of the total composite mix are introduced. In an attempt of developing SHCCs with relatively low fiber volume fraction, the steady-state crack opening theory was applied to the case of short randomly dispersed fibers in a brittle-matrix [9-11]. This theory was originally developed by Marshal and Cox [12] for cement and ceramic matrices reinforced with continuous fibers. Based on this theory, the steady-state crack opening theory was proposed to assess analytically the potential of flat crack propagation when the crack's surrounding medium is submitted to a constant stress field. The essential condition to occur a steady-state crack opening is that the complementary energy J_b provided by the fibers bridging work should be higher or equal to the crack tip fracture toughness J_{ip} :

$$J_{ip} \leq \sigma_p \delta_p - \int_0^{\sigma_p} \sigma(\delta) \equiv J_b \quad (1)$$

For composites with low fibers volume fraction, $J_{ip} = K_m^2 / E_m$ where K_m and E_m are the matrix fracture toughness [13] and young's modulus, respectively (Figure 1).

Li et al. [14] showed that for a composite with a volume fraction V_f of discrete fibers, the fiber bridging stress versus crack opening ($\sigma_B - \delta$) curve can be predicted by integrating over the contribution of those fibers that cross the matrix crack plane:

$$\sigma_B(\delta) = \frac{4V_f}{\pi d_f^2} \int_{\phi=0}^{\pi/2} \int_{z=0}^{(L_f/2)\cos\phi} P(\delta) p(\phi) p(z) dz d\phi \quad (2)$$

where L_f is the fiber length, d_f is the fiber diameter, $p(\phi)$ and $p(z)$ are probability density functions of the orientation angle and centroidal distance of fibers from the crack plan, respectively.

Assuming that all the fibers are aligned to the tensile loading direction, and all the fibers will fully pull out under a constant frictional bond between fiber and matrix during (τ_0), Equation 2 can be simplified as [15]:

$$\sigma_B(\delta) \begin{cases} 2V_f \sqrt{(2G_d + \tau_0 \delta) \frac{E_f}{d_f} - \frac{V_f E_f \delta}{L_f}} & \delta \leq \delta_c \\ \frac{4V_f \tau_0}{L_f d_f} \left(\frac{L_f}{2} - \delta \right)^2 & \delta < \delta_c < \frac{L_f}{2} \end{cases} \quad (3)$$

where E_f is the fiber's modulus of elasticity and G_d is the energy required for fibers being fully debonded along their embedded length (chemical bond).

Integrating equation (3) based on the definition of the complementary energy as shown in Fig. 1, and indicated analytically in equation (1), J_b can be obtained from:

$$J_b = \frac{V_f L_f}{d_f} \left(\frac{\tau_0^2 L_f^2}{6d_f E_f} - 2G_d \right) \quad (4)$$

Neglecting the chemical bond G_d that is valid for the case of hydrophobic fibers, and replacing equation (4) in (1), the critical fibers volume fraction ($V_{f,crit}$) to achieve a strain hardening response for a given fiber, matrix and fiber/matrix interface properties can be theoretically obtained from:

$$V_{f,crit} = \frac{6d_f^2 E_f}{\tau_0^2 L_f^3} J_{tip} \quad (5)$$

Using the knowledge derived from this micro-mechanical model, Li and co-workers [16, 17] tailored and introduced practically the synthetic fibers as the discrete reinforcement to a cementitious matrix. To the resulting material the designation Engineered Cementitious Composite (ECC) was attributed. Only 2% in volume of Polyethylene Spectra-900 (PE), a polymeric fiber with high modulus of elasticity (120 GPa) and tensile strength (2600 MPa), has provided a strain hardening capacity of 3.5% to its original brittle cement based matrix. Further, the Plasma treatment of PE fibers increased the frictional bond strength almost two times, upgrading the composite strain ductility to 7%, while a tensile strength of 6 MPa was achieved [18, 19].

The initial efforts to develop a SHCC utilizing Polyvinyl Alcohol (PVA) fibers was resulted in a composite with a maximum strain capacity of around 0.5% [20-22], By using this micromechanical approach, and considering the effect of the chemical bond, Li et al. [23] have successfully developed a very ductile PVA-ECC by modifying both the matrix and the fiber/matrix interface.

In fact, the presence of the hydroxyl group in the molecular chains of the hydrophilic PVA fibers provides a strong chemical bond with surrounding hydrated cement particles. This strong chemical

bond proportionates a further increase in the frictional fiber pullout resistance due to the bonded matrix particles to the fiber surface. However, as equation (4) shows, the complementary energy J_b decreases by increasing the chemical bond G_d . A too high chemical bond G_d can also lead to premature fiber rupture during debonding or pulling out.

Polymeric fibers present a slip-hardening pullout response due to the fibrillation. This slip-hardening response is being introduced in analytical models by a slip-hardening parameter (β). For the case of PVA fibers a pronounced slip-hardening response during fiber pullout was observed that leads to the premature fiber failure in shear-delamination mode [24, 25]. The general profile of a single fiber pullout curve is shown in Fig. 2.

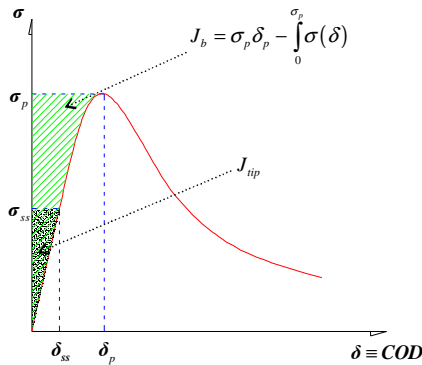


Figure 1: Typical $\sigma(\delta)$ for strain hardening composites; J_b is the complementary energy and J_{tip} is the crack tip fracture toughness, σ_{ss} and δ_{ss} are stress and its crack opening at the steady-state crack formation.

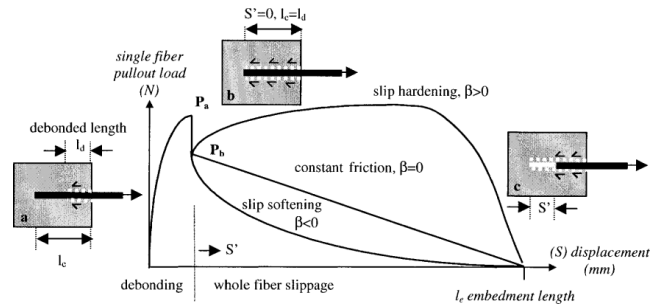


Figure 2: General profile of a single fiber pullout curve [25].

Coating of the fiber surface with a proper agent can reduce effectively the hydrophilic character of PVA fibers by controlling the interface bond and slip-hardening. Redon et al. [23] and Li et al. [25, 26], have attempted to tailor the interface of PVA fibers utilizing different quantities (based on fiber's weight ratio) of an oiling agent. The results of the both pullout tests and tensile test on composites indicated that utilizing 1.2% of this coating can optimize the interface of PVA/cement-matrix for developing tight enough saturated multiple cracking (stabilized crack formation process). $G_d < 2.2 \text{ J/m}^2$; $\tau_0 = 1.0\text{-}1.2 \text{ MPa}$; and $\beta < 1.5$ were taken as the optimal ranges of values for the tailoring of PVA-fiber/matrix interface bond. These values were obtained by Wu [27] using an available fiber-bridging model [28] and adopting $J_{tip} = 5 \text{ J/m}^2$.

The use of high volume fraction of fly ash is another alternative to reduce both the PVA fiber/matrix interface bond and matrix crack tip toughness J_{tip} [29, 30]. Therefore fly ash not only can increase the J_b , but also decrease J_{tip} , providing much safer margin for the formation of saturated crack patterns, in consequence of the increase of J_b/J_{tip} ratio [31].

Replacing cement by high volume of fly ash leads to a decrease of the costs of ECC and to an increase of the sustainability of the material [32], as well as the enhancement of the micro-mechanical properties of these composite materials.

Although the long term performance and durability of ECC under different loading conditions such a freeze-thaw cycles, carbonation exposure, hot-cold temperature cycles, fatigue loading, and long term mechanical performance are well studied [33-36], no information was found in the literature dealing with the curing conditions on the mechanical behavior of this material.

It is speculated that different curing conditions could affect both fiber/matrix interface properties and matrix toughness. To contribute for the knowledge in this topic, an experimental research program was conducted to study PVA-ECCs tensile behavior when this composite is cured under different

conditions. The results derived from the fibers-bridging stress versus crack opening, along with microscopic photos, are used to investigate this effect.

2 EXPERIMENTAL PROGRAM

2.1 Materials

The PVA fiber used in this study was produced by Kuraray Company and is designated RECs15x8. Both mechanical and geometrical properties of this fiber are presented in Table 1. The matrix was composed of fly ash, cement, sand, water and chemical admixtures.

Table 1: Properties of PVA fiber

Fiber Type	Diameter	Length	Nominal tensile strength	Apparent tensile strength	Modulus of elasticity	Density	Elongation
	μm	mm	MPa	MPa	GPa	gr/cm^3	%
PVA RECs15x8	40	8	1600	1092	40	1.3	7

*The tensile strength of fiber embedded in cementitious matrix.

The chemical composition of the fly ash complies with the minimum requirements indicated in EN-450 [37] for being used as a partial replacement of cement in concrete. Based on this standard the fly ash was categorized in class B and group N for the loss of ignition and fineness, respectively. The properties and the chemical composition of the used fly ash are indicated in Table 2. Type I 42.5R Portland cement with a specific gravity of $3.15 \text{ gr}/\text{cm}^3$ and, silica sand with a maximum grain size of $500\mu\text{m}$ and specific density of $2.63 \text{ gr}/\text{cm}^3$ were the other dry ingredients of the mix composition. The mix proportions and procedures are presented in Table 3 and Table 4, respectively.

Table 2: Fly ash properties and chemical composition

specific gravity	Cl ⁻	SO ₃	CaO Free	CaO reactive	SiO ₂ reactive	SiO ₂ + Al ₂ O ₃ + Fe ₂ O ₃	MgO	P ₂ O ₅	Total alkalis	Retained on No. 325 sieve	I.A. _{28D} *	I.A. _{90D} **
gr/cm^3	%	%	%	%	%	%	%	%	%	%	%	%
2.42	0	0.12	0.1	2.7	40.8	89.9	1.9	1.92	0.25	15	79	99

* Strength activity index with Portland cement at 28 days; ** Strength activity index with Portland cement at 90 days.

2.2 Specimen configuration and preparation

Four similar panels of a size of $490 \times 500 \times 20 \text{ mm}^3$ were produced by casting the prepared composite inside the acrylic moulds. For the casting purpose, a standard slump cone executed in order to also verify the capacity of obtaining a homogenous spreading, characteristic of a self compacting material, as well as the ability of the material to fill the mould under its own weight (Figure 3a). The same casting process was adopted in the four panels. The composite was flowed homogeneously, and a circular shape was maintained until reaching the extremities of the mold (Figure 3b). Since the rheological characteristics of the developed ECC were tailored to have self consolidating requisites, the corner of the mould was easily filled up without the need to any external vibration. Each panel was built with a batch of composite of around five liters, and this filling process of the mould was applied to all the panels.

Table 3: Composite mix proportions based on weight ratio percentage

Fly ash / Cement	Water / B*	Sand / B*	Admixtures/B*	PVA fibers**
120	30	50	2.2	2

* B: Binder (cement + fly ash)

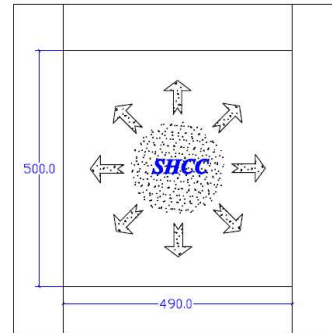
** Percentage of total composite mix volume.

Table 4: Composite mix procedure

Steps	Mix ingredients for each step	Duration (sec)
Step 1	Sand + Cement + Fly Ash	30
Step 2	1/2 (water + admixtures)	150
Step 3	1/2 (water + admixtures)	150
Step 4	PVA-Fibers	300



a)



b)

Figure 3: Casting ECC panels: a) using slump cone for casting; b) the self-compacting composite was spread diagonally maintaining high homogeneity for the casted panels (dimensions in mm).

Just after the panels have been cast, they were sealed with a plastic sheet and were kept in a room temperature during 24 hours before de-molding, in order to prevent loss of hydration moisture in the early age. After de-molding, all the specimens were cured in a constant temperature equal to 20°C, but in different humidity conditions up to the age of 28 days. The panels designated SL1 and SL4 were cured in constant relative humidity of 57% and 85%, respectively. The SL3 panel was immersed inside a water container. To verify the effect of humidity change at the early age, the SL2 panel was cured in a humidity of 57% up to the age of 8 days and then moved to a room of 85% humidity and was cured there up to 28 days. These curing conditions of the panels are presented in Table 5.

It should be noted that, to cut the tensile specimens from the panels, all of them were taken out at the age of 14 days for few hours and, after cutting, they were cured again in their previous controlled conditions. The panels were cut according to the arrangement represented in Figure 4a by using a diamond saw machine. From each panel, 10 specimens of two different sizes were extracted. All specimens have a width of 70 mm, but the specimens 1 to 6, and 7 to 10 had a length of 370 mm and 244 mm, respectively.

To study the single crack opening behavior a notch was executed in each lateral side at half of the length of specimens 7 to 10. The geometry of this notch is indicated in Fig. 4b. The specimens 1 to 6 were prepared to study the influence of curing conditions on multiple cracking of PVA-ECCs response, which is out of the scope of this paper.

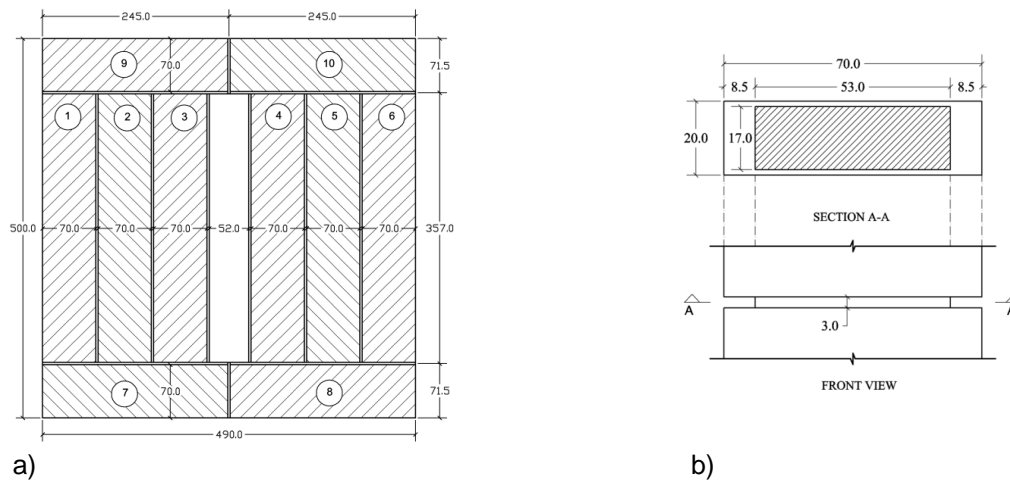


Figure 4: a) Cutting pattern of the tensile rectangular specimens from the panels; b) notch geometry (dimensions in mm).

Table 5: Curing details for the PVA-ECC panels

Panels	First 24 hours	Up to the Age of 8 days	Up to the age of 28 days
SL1	Sealed in room temp.	20° C, 57% humidity	20° C, 57% humidity
SL2	Sealed in room temp.	20° C, 57% humidity	20° C, 85% humidity
SL3	Sealed in room temp.	Immersed in water at 20° C	Immersed in water at 20° C
SL4	Sealed in room temp.	20° C, 85% humidity	20° C, 85% humidity

2.3 Test Setup

One day before testing, the specimens were removed from their imposed curing conditions, and were kept in the room temperature to get dry. The tests were performed in a servo-controlled machine equipped with a load-cell of 200 kN. Two wedge grips secured the specimen providing to the specimen clamped ends conditions. The crack opening displacement (COD) was measured using four LVDTs (Figure 5) mounted in a device that was conceived and built in order to measure the in plane and the out-of-plane rotation of the specimen. Another external LVDT was used to control the test, by imposing a displacement rate of 5 $\mu\text{m}/\text{sec}$. The test was stopped when the COD has exceeded 2.5 mm.

3 RESULTS AND DISCUSSION

The results of the tests will be discussed in terms of the influence of the curing conditions on (Figure 6): the discrepancy of σ_B -COD response; average normal stress at crack initiation (σ_{cr}); average maximum fibers bridging stress (σ_p) and its corresponding crack opening (COD_p); average absorbed energy up to $COD=2.5$ mm ($G_{f,2.5}$); average absorbed energy up to COD_p ($G_{f,p}$); and average absorbed energy in the post peak regime up to the $COD=2.5$ mm ($G_{f,PP}$), and the fibers bridging stiffness. The absorbed energy is calculated by integrating the area under the σ_B -COD up to a certain COD (Figure 6).

The average and envelop of the σ_B -COD responses of the four specimens (except of SL4) are presented in Figure 7. The results related to the SL4 panel are only corresponding to three specimens, due to the deficient functioning of the equipment when installing one specimen. The dispersion in the response of the ECC is generally due to the randomness sources such as interfacial bond properties,

three-dimensional fibers orientation and distribution, and also the disorder nature of flaws (weak cement/aggregates bond or air voids) that affect the matrix toughness.



Figure 5: Tensile test setup for notched specimen

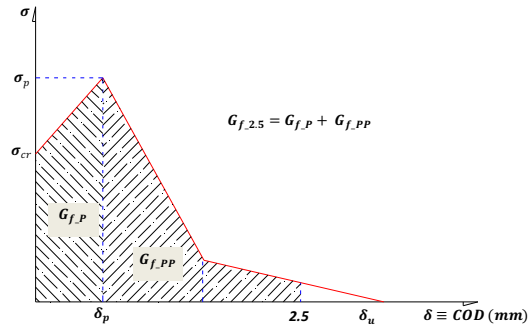


Figure 6: Three linear diagram for the simulation of the fiber bridging stress versus crack opening response, and meaning of the determined parameters

From Figure 7, it is verified that SL4 has the lower and SL3 has the higher amount of discrepancy for the σ_B -COD responses. The dispersion of the results of SL2 and SL1 is in the interval of the dispersion of the results of the other two series of specimens. It might be concluded that, although the curing with higher humidity seems to significantly reduce the randomness in terms of fiber bridging response, the curing in water seems to have the inverse effect.

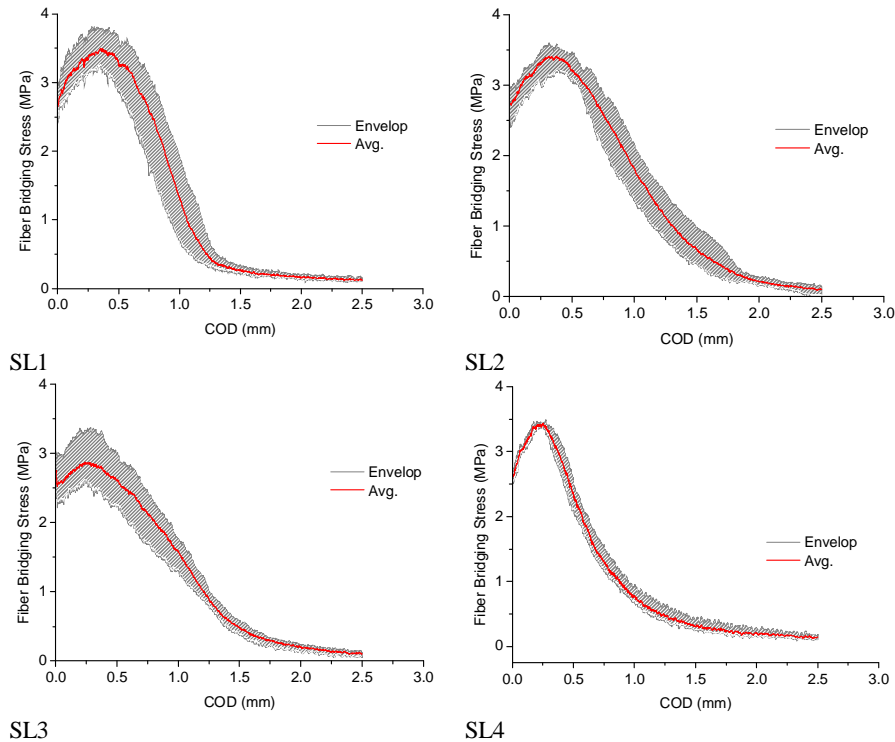


Figure 7: The average and the envelope of σ_B -COD for specimens SL1 to SL4.

The results derived from σ_B -COD are indicated in Table 6 and represented graphically in Figure 8. The stress at cracking initiation, σ_{cr} , for all the specimens has almost the same values that have ranged from 2.63 to 2.74 MPa corresponding to SL3 and SL4, respectively.

Table 6: Data obtained from average of σ_B -COD for specimens SL1 to SL4.

Specimen	σ_{cr}	COD_P	σ_P	$G_{f_{2.5}}$	G_{f_P}	$G_{f_{PP}}$
-	(MPa)	(mm)	(MPa)	(N/mm)	(N/mm)	(N/mm)
SL1	2.64	0.376	3.55	3.343	1.213	2.130
SL2	2.73	0.341	3.46	3.741	1.053	2.688
SL3	2.74	0.247	2.92	3.127	0.682	2.445
SL4	2.63	0.250	3.47	2.666	0.670	1.996

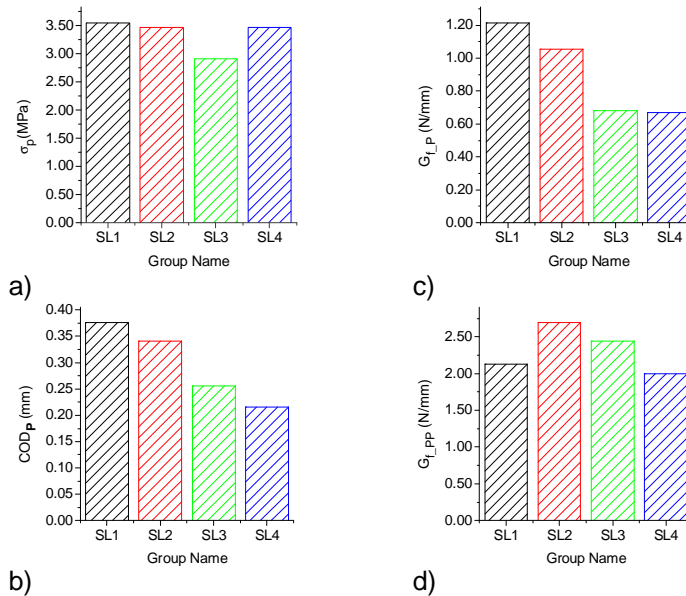


Figure 8: Graphical representation of the results derived from the σ_B -COD: a) σ_p , b) COD_P , c) G_{f_P} , d) $G_{f_{PP}}$.

The maximum bridging stress, σ_p , for SL1, SL2 and SL4 is almost close to 3.50 MPa, while a reduction about 20% was registered in the SL3 that was cured immersed into water. However, the crack opening at σ_p (COD_P) for all the specimens can be ordered from the smaller to the larger crack width in the following sequence: SL4, SL3, SL2 and SL1. As shown in Figure 9a, the smaller COD_P along with high σ_p , presented by SL4, provided the highest bridging stiffness in the hardening branch when compared to the other specimens. In spite of a relatively small COD_P , the SL3 has presented the lowest bridging stiffness (the slope of the phase between crack initiation and COD_P) due to its smaller σ_p . Figure 9a shows that SL1 and SL2 have also presented a bridging stiffness similar to the value shown by SL4. This figure also shows that the SL4 has presented the highest tensile stress decay during the post-peak softening phase, while the opposite was observed in the SL2.

Photos of the fibers in fracture surface with a zoom magnitude of 400X revealed that, although the majority of the fibers of SL1, SL2 and SL4 have ruptured in a thin pencil shape end configuration, the major part of the fibers of SL3 seems to be pulled out (Figure 10). Also the shorter pulled out length for

the majority of the fibers in the fracture section of SL4 when compared to the other specimens, is in full agreement with its smaller COD_P and with the higher bridging stiffness in the hardening regime (Fig. 11). This can be justified by the stronger fiber/matrix interface bond. The more abrupt softening branch in the SL4 can also be reasonably justified with the rupture of the most of the fibers in hardening branch.

In terms of $G_{f_{2.5}}$, SL2 and SL4 have presented the highest and the lowest value, 3.74 N/mm and 2.67 N/mm, respectively, Table 6 and Figure 9b. Figure 8 indicates that SL1 and SL2 have absorbed the highest amount of energy corresponding to G_{f_P} and $G_{f_{PP}}$, respectively.

Referring to the Figure 8b, SL1, SL2 and SL4 have the same evolution for the energy absorption up to a crack opening around 400 μm (a little above the COD_P). Although the potential of energy absorption for SL3 is lower than SL4 for tighter cracks, after a $COD=750 \mu\text{m}$ the SL3 has much higher rate for energy absorption.

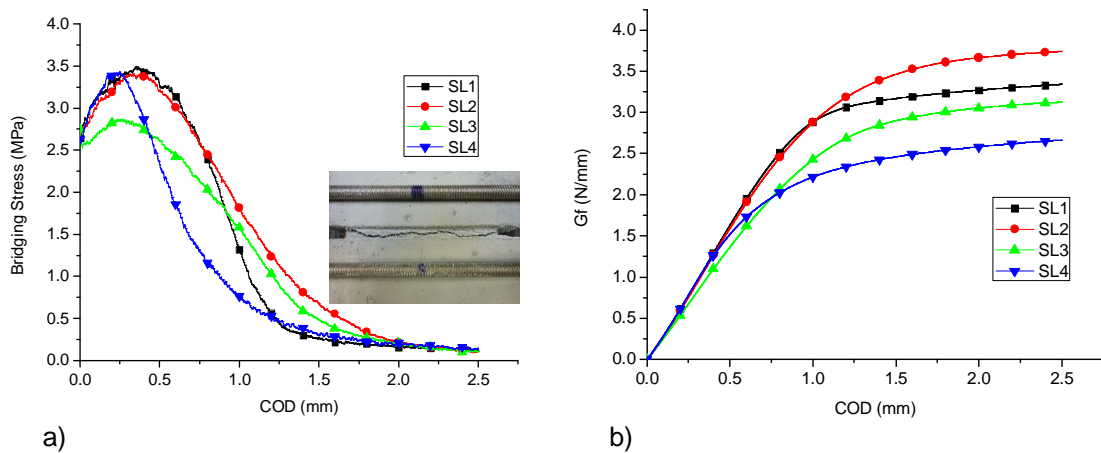


Figure 9: a) Crack opening displacement versus fiber bridging stress and the typical observed crack, b) absorbed energy for the specimens tested under different curing conditions.

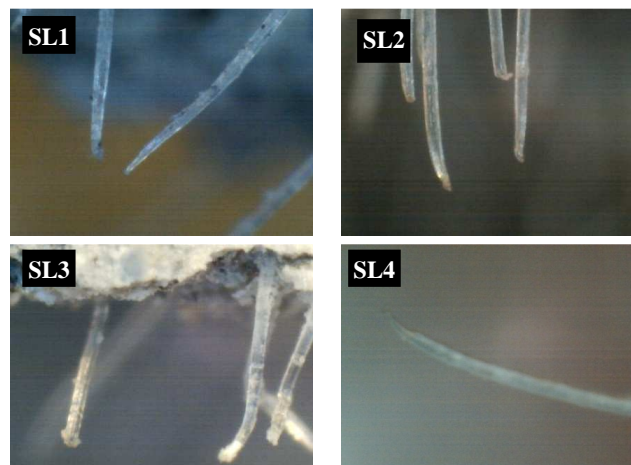


Figure 10: Fiber failure modes at the fracture section of the specimens (zoom magnitude: 400X).

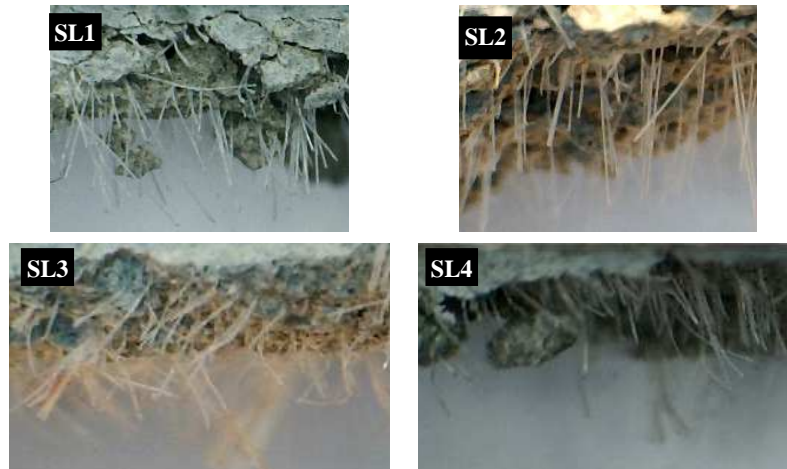


Figure 11: Photos of the fibers bridging the fracture surface of typical specimens of the tested panels (zoom magnitude: 200X).

4 CONCLUSIONS

In this paper direct tensile tests with notched PVA-ECC specimens extracted from panels subjected to four different curing conditions were executed in order to assess the influence of these conditions on the single crack opening behavior of these composites.

The curing conditions seem do not have affected the stress at crack initiation. Up to a crack width of around 0.3 mm, which is the maximum allowed by design standards for reinforced concrete structures, all the specimens have, in general, presented a tensile strain hardening phase. However, the specimens were cured immersed into water have shown the lowest peak tensile strength, and, therefore, they have presented the lowest stiffness in this hardening phase.

The specimens cured at higher humidity have conducted to the smallest crack width at the peak tensile strength, but the lowest energy absorbed in the fracture process up to a crack width of 2.5 mm. Therefore, the high humidity curing conditions seem to provide benefits in terms of durability since cracks of smaller width can be obtained during the strain hardening phase of the corresponding composite. The specimens submitted to these curing conditions have also presented the lowest scatter in terms of stress-crack width response. However, the high humidity curing conditions seem to have a detrimental effect in terms of energy absorption capacity that might have been caused by the rupture of a high number of fibers in consequence of the highest stiffness of this composite in its strain hardening phase.

Curing in lower humidity for the early ages (8 days) and then under the higher humidity up to 28 days, resulted in higher energy absorption up to a crack opening of 2.5 mm.

It is speculated that the fibers/matrix chemical bond and the use of relatively high volume fraction of fly ash are the main reasons for this high level of sensitivity of PVA-ECCs tensile response to the curing conditions. Fly ash not only could affect the fibers/matrix chemical bond by its reaction with cement by-products, but also could change the geometrical structure of this interface zone. This also could lead to the change in the slip-hardening response of the pulled out fibers.

Since the rate of the chemical reaction and, with a consequent smaller increase of strength development, is lower for mortars containing fly ash when compared to those just with cement, it is important to extend this study to specimens of higher age (at least 90 days).

The assessment of the single fiber pullout behavior, and micro-scale observations by SEM could be further helpful for a deeper understanding of the effect of the curing conditions on the post-cracking behavior of these composites.

ACKNOWLEDGEMENTS

The study presented in this paper is a part of the research project titled "PrePam –Pre-fabricated thin panels by using advanced materials for structural rehabilitation" with reference number of PTDC/ECM/114511/2009. The first author acknowledges the grant SFRH/BD/65663/2009 provided by FCT. The authors also thank the collaboration of the following companies: Sika for providing the sand, Grace for the superplasticizers, Dow Chemical Co. for viscous modifying agents and SECIL for supplying the cement.

REFERENCES

- [1] M.D. Prisco, D. Dozio and M. Colombo, "On the Bearing Capacity of FRC Structures: Is the Material Characteristic Value the Right Choice?", 2nd International RILEM Conference on Strain Hardening Cementitious Composites (SHCC2), Rio de Janeiro, Brazil, 279-288, Dec 12-14, 2011.
- [2] J.A.O. Barros, E. Esmaeeli, E. Manning and D. Häßler, "Flexural Strengthening of Masonry Members Using Advanced Cementitious Materials", 2nd International RILEM Conference on Strain Hardening Cementitious Composites (SHCC2), Rio de Janeiro, Brazil, 279-288, Dec 12-14, 2011.
- [3] R.F. Correia, E.M.R. Fairbairn, R.D.T. Filho and C.R. Miranda, "Structural behavior of SHCC cement sheath in oil well submitted to steam injection: experimental analysis", 2nd International RILEM Conference on Strain Hardening Cementitious Composites (SHCC2), Rio de Janeiro, Brazil, 279-288, Dec 12-14, 2011.
- [4] G. Fischer, H. Fukuyama and V.C. Li, "Influence of Matrix Ductility on Tension-Stiffening Behavior of Steel Reinforced Engineered Cementitious Composites (ECC)", *ACI Structural Journal*, 99(1), 104-111 (2002).
- [5] B.L. Karihaloo, F.J. Alaei and S.D.P. Benson, "A new technique for retrofitting damaged concrete structures", *Proceedings of the ICE - Structures and Buildings*, 309–318, 2002.
- [6] S.D.P. Benson and B.L. Karihaloo, "CARDIFRC - Manufacture and Constitutive Behaviour", A.E. Naaman and H.W. Reinhardt, 4th International RILEM Workshop on High Performance Fiber - Reinforced Cement Composites (HPFRCC4), RILEM Publications S.A.R.L, 65-79, 2003.
- [7] G. Chanvillard and S. Rigaud, "Complete Characterisation of Tensile Properties of DUCTAL® UHPFRC According to the French Recommendations", A.E. Naaman and H.W. Reinhardt, 4th International RILEM Workshop on High Performance Fiber - Reinforced Cement Composites (HPFRCC4), RILEM Publications S.A.R.L, 65-79, 2003.
- [8] A.E. Naaman and J.R. Homrich, "Tensile Stress-Strain Properties of SIFCON", *ACI Materials Journal*, 86(3), 244-251 (1989).
- [9] C.K.Y. Leung and V.C. Li, "New Strength-Based Model for the Debonding of Discontinuous Fibres in an Elastic Matrix", *J. of Material Science*, 26, 5996-6010 (1991).
- [10] V.C. Li and C.K.Y. Leung, "Steady State and Multiple Cracking of Short Random Fiber Composites", *ASCE J. of Engineering Mechanics*, 18, 2246-2264 (1992).
- [11] V. Li and H.C. Wu, "Conditions for pseudo strain hardening in fiber reinforced brittle matrix composites", *Applied Mechanics Reviews*, 45(8), 390–398 (1992).
- [12] D.B. Marshall and B.N. Cox, "A J-integral Method For Calculating Steady-State Matrix Cracking Stress in Composites.", *Mechanics of Materials*, 7(8), 127-133 (1988).
- [13] J.G.M.V. Mier, *Fracture Processes of Concrete: Assessment of Material Parameters for Fracture Models*, 1 ed., CRC-Press, (1997).
- [14] V.C. Li, Y. Wang and S. Backer, "A micromechanical model of tension softening and bridging toughening of short random fiber reinforced brittle matrix composites.", *J. Mech. Phys. Solids*, 39(5), 607-625 (1991).
- [15] S. Wang, "Micromechanics Based Matrix Design for Engineered Cementitious Composites." Ann Arbor, USA: University of Michigan; 2005.
- [16] V.C. Li, D.K. Mishra and H.C. Wu, "Matrix Design for Pseudo Strain-Hardening Fiber Reinforced Cementitious Composites", *RILEM Journal Materials and Structures*, 28(183), 586 - 595 (1995).

- [17] H.C. Wu and V.C. Li, "Trade-off between strength and ductility of random discontinuous fiber reinforced cementitious composites", *J. of Cement and Concrete Composites*, 16, 23-29 (1994).
- [18] V.C. Li, H.C. Wu and Y.W. Chan, "Effect of plasma treatment of polyethylene fibers on interface and cementitious composite properties", *J. of American Ceramic Society*, 79(3), 700-704 (1996).
- [19] V.C. Li, H.C. Wu and Y.W. Chan, Interface Property Tailoring for Pseudo Strain-Hardening Cementitious Composites, in: G.C. Sih, A. Carpinteri and G. Surace (Eds.) *Advanced Technology for Design and Fabrication of Composite Materials and Structures*, Kluwer Academic Publishers, Netherland, 1995, pp. 261-268.
- [20] Y. Shao and S.P. Shah, "Mechanical Properties of PVA Fiber Reinforced Cement Composites Fabricated by Extrusion Processing", *ACI Materials Journal*, 94(6), 555-564 (1997).
- [21] L.R. Betterman, C. Ouyang and S.P. Shah, "Fiber-Matrix Interaction in Microfiber-Reinforced Mortar", *Advanced Cement Based Materials*, 2(2), 53-61 (1995).
- [22] S.P. Shah, A. Peled, C.M. Aldea and Y. Akkaya, "Scope of high performance fiber reinforced cement composites", H.W. Reinhardt and A.E. Naaman, *Third International RILEM Workshop on High Performance Fiber Reinforced Cement Composites*, RILEM Publications SARL, 113 -129, 1999.
- [23] V.C. Li, W. Shuxin and C. Wu, "Tensile Strain-hardening Behavior of Polyvinyl Alcohol Engineered Cementitious Composite (PVA-ECC)", *ACI Materials Journal*, 98(6), 483-492 (2001).
- [24] T. Kanda and V.C. Li, "Interface Property and Apparent Strength of High Strength Hydrophilic Fiber in Cement Matrix", *ASCE J. Materials in Civil Engineering*, 10(1), 5-13 (1998).
- [25] C. Redon, V.C. Li, C. Wu, H. Hoshiro, T. Saito and A. Ogawa, "Measuring and Modifying Interface Properties of PVA Fibers in ECC Matrix", *ASCE J. Materials in Civil Engineering*, 13(6), 399-406 (2001).
- [26] V.C. Li, C. Wu, A. Ogawa and T. Saito, "Interface Tailoring for Strain-hardening PVA-ECC", *ACI Materials Journal*, 99(5), 463-472 (2002).
- [27] C. Wu, "Micromechanical Tailoring of PVA-ECC for Structural Applications." Ann Arbor, USA: University of Michigan; 2001.
- [28] Z.T. Lin, Kanda and V.C. Li, "On Interface Property Characterization and Performance of Fiber Reinforced Cementitious Composites", *J. Concrete Science and Engineering*, RILEM, 1, 173-184 (1999).
- [29] S.F.U. Ahmed and M. Maalej, "Fracture Toughness of Cement Mortar Containing High Volume Fly Ash", *ACI Special Publication*, 242, 321-332 (2007).
- [30] A. Peled, M.F. Cyr and S.P. Shah, "High Content of Fly Ash (Class F) in Extruded Cementitious Composites", *ACI Materials Journal*, 97(5), 509-517 (2000).
- [31] S. Wang and V.C. Li, "Engineered cementitious composites with high-volume fly ash," *ACI Materials Journal*, 104, 233-241 (2007).
- [32] E.H. Yang, Y. Yang and V. Li, "Use of High Volumes of Fly Ash to Improve ECC Mechanical Properties and Material Greenness", *ACI Materials Journal*, 104(6), 620-628 (2007).
- [33] M.D. Lepech and V.C. Li, "Long Term Durability Performance of Engineered Cementitious Composites", *J. of Restoration of Buildings and Monuments*, 12(2), 119-132 (2006).
- [34] W.P. Boshoff and G.P.a.G.V. Zijl, "Time-dependent response of ECC: Characterisation and modeling of creep and creep fracture", *Workshop on HPFRCC in Structural Applications*, Honolulu, Hawaii, USA, 125-134, 2005.
- [35] J. N`Eme`Cek, P. Kabele, L. Kopecký and Z. Bittnar, "Effect of chemical exposure on fiber reinforced cementitious matrix", *SEMC 2007, the Third International Conference on Structural Engineering, Mechanics and Computation*, Cape Town, South Africa, Sep 10-12, 2007.
- [36] F.H. Wittmann, P. Wang, P. Zhang, T. Zhao and F. Beltzung, "Capillary Absorption and Chloride Penetration into Neat and Water Repellent SHCC under Imposed Strain", *2nd International RILEM Conference on Strain Hardening Cementitious Composites (SHCC2)*, Rio de Janeiro, Brazil, 165-172, Dec 12-14, 2011.
- [37] E. Standard, Fly ash for concrete, in: Part 1: Definition, specifications and conformity criteria, European Committee for Standardization, 2005.